frontiers in Earth Science

ORIGINAL RESEARCH
published: 23 April 2018
doi: 10.3389/feart.2018.00030

Textural Insights Into the Evolving Lava Dome Cycles at Santiaguito Lava Dome, Guatemala

Emma Rhodes[1], Ben M. Kennedy[1], Yan Lavallée[2], Adrian Hornby[2,3], Matt Edwards[1] and Gustavo Chigna[4]*

[1] Geological Sciences, University of Canterbury, Christchurch, New Zealand, [2] Department of Earth, Ocean and Ecological Sciences, University of Liverpool, Liverpool, United Kingdom, [3] Earth and Environmental Sciences, Ludwig-Maximilian University of Munich, Munich, Germany, [4] Instituto Nacional de Sismologia, Vulcanologia, Meteorologia, e Hydrologia, Guatemala City, Guatemala

OPEN ACCESS

Edited by:
Jacob B. Lowenstern, Cascades Volcano Observatory (CVO), Volcano Disaster Assistance Program (USGS), United States

Reviewed by:
Sonia Calvari, Istituto Nazionale di Geofisica e Vulcanologia (INGV), Italy
Michelle Lynn Coombs, Alaska Volcano Observatory (AVO), United States

***Correspondence:**
Emma Rhodes
nzemmarhodes@gmail.com

Specialty section:
This article was submitted to Volcanology, a section of the journal Frontiers in Earth Science

Received: *02 November 2017*
Accepted: *16 March 2018*
Published: *23 April 2018*

Citation:
Rhodes E, Kennedy BM, Lavallée Y, Hornby A, Edwards M and Chigna G (2018) Textural Insights Into the Evolving Lava Dome Cycles at Santiaguito Lava Dome, Guatemala. Front. Earth Sci. 6:30. doi: 10.3389/feart.2018.00030

The structures and textures preserved in lava domes reflect underlying magmatic and eruptive processes, and may provide evidence of how eruptions initiate and evolve. This study explores the remarkable cycles in lava extrusion style produced between 1922 and 2012 at the Santiaguito lava dome complex, Guatemala. By combining an examination of eruptive lava morphologies and textures with a review of historical records, we aim to constrain the processes responsible for the range of erupted lava type and morphologies. The Santiaguito lava dome complex is divided into four domes (El Caliente, La Mitad, El Monje, El Brujo), containing a range of proximal structures (e.g., spines) from which a series of structurally contrasting lava flows originate. Vesicular lava flows (with a'a like, yet non-brecciated flow top) have the highest porosity with interconnected spheroidal pores and may transition into blocky lava flows. Blocky lava flows are high volume and texturally variable with dense zones of small tubular aligned pore networks and more porous zones of spheroidal shaped pores. Spines are dense and low volume and contain small skeletal shaped pores, and subvertical zones of sigmoidal pores. We attribute the observed differences in pore shapes to reflect shallow inflation, deflation, flattening, or shearing of the pore fraction. Effusion rate and duration of the eruption define the amount of time available for heating or cooling, degassing and outgassing prior to and during extrusion, driving changes in pore textures and lava type. Our new textural data when reviewed with all the other published data allow a cyclic model to be developed. The cyclic eruption models are influenced by viscosity changes resulting from (1) initial magmatic composition and temperature, and (2) effusion rate which in turn affects degassing, outgassing and cooling time in the conduit. Each lava type presents a unique set of hazards and understanding the morphologies and dome progression is useful in hazard forecasting.

Keywords: lava dome, Santiaguito, pore structure, effusion rate, degassing

INTRODUCTION

The morphology and textures of lava preserve a story of the conditions and processes taking place during its ascent. Recognizing and understanding conditions for various extrusive and eruptive products can provide insights to future timing of events and associated hazards (Calder et al., 2015). At lava domes worldwide, lava morphology and surface textures have been shown to form in response to several emplacement variables, including variations in effusion rate (Watts et al., 2002), emplacement stress regime (Fink et al., 1990; Hale and Wadge, 2008), changes in volatile content (Anderson and Fink, 1990), crystallinity or composition (Watts et al., 2002), fragmentation processes (Wadge et al., 2009), and sintering (Kendrick et al., 2016). Insights into the interacting variables are preserved in the crystal and pore textures of the lava and further supplemented by compositional analysis and observations during eruption. At dome volcanoes, the volatile content, and consequently bubbles, are considered particularly important as the system is often on the boundary between explosive and effusive behavior (e.g., Edmonds and Herd, 2007; Mueller et al., 2011).

Bubbles are considered stationary rather than mobile in highly-crystalline high viscosity magmas, as the viscous forces dominate over the buoyant forces acting on the bubbles, promoting a coupled rise of melt and bubbles (Sparks, 2003). Where magma is rising slowly, permeable magma foam (Eichelberger et al., 1986; Jaupart and Allègre, 1991; Rust and Cashman, 2011), or cracked magma (Tuffen et al., 2003; Lavallée et al., 2013) allows outgassing along the outer shear margin of the magmatic column (Gaunt et al., 2014; Hornby et al., 2015) and/or out into the surrounding country rock, developing a partially or periodically open system (Castro et al., 2012; Cashman and Sparks, 2013; Kendrick et al., 2013). Evidence of continual outgassing and a periodically open system can both be observed at Santiaguito (Stoiber and Rose, 1969; Bluth and Rose, 2004; Johnson, 2004; Holland et al., 2011; Scharff et al., 2012; Ball et al., 2013).

Here we consider degassing as the shallow process of volatiles exsolving from the melt—typically forming bubbles (pores). This process is controlled by the volatile overpressure and solubility, and equilibrium conditions permitting bubble nucleation and growth (Cashman and Sparks, 2013). In contrast, we view outgassing as the process of the exsolved volatiles escaping from the lava, which requires a permeable pathway. A prerequisite for the effusion of high-viscosity lava domes is the partial development of open system degassing and outgassing (Calder et al., 2015). In an open system, gas is able to escape from the magma, reducing gas pressure and decreasing the chance of explosive eruptions (Cashman et al., 2000; Gonnermann and Manga, 2007; Holland et al., 2011; Mueller et al., 2011). Both degassing and outgassing are affected by temperature, pressure, stress conditions, and the residence time of magma in the shallow conduit. In particular, residence time in the conduit is important for high-viscosity magmas for which the physical processes associated with bubble growth, coalescence, and collapse, is sluggish.

Santiaguito comprises four domes (El Caliente, La Mitad, El Monje, El Brujo) which are aligned along an overall E-W trend (**Figure 1**). Extrusion began in 1922, and has continued uninterrupted, with nine documented cycles of extrusion (Rose, 1973b; Harris et al., 2003; Ebmeier et al., 2012). Santiaguito has experienced a range of activity during this time including lava dome, lava flow, and spine extrusions. Extrusive activity is punctuated by explosive events which has resulted in Vulcanian gas- and ash-plumes (**Figure 1A**) and occasionally pyroclastic density currents. El Caliente vent is the only site to have been continuously active since 1922. The three other domes are mostly inactive, except for mild gas emission, and are thus accessible for textural analysis. Evolution of the domes has been extensively described and documented (Sapper, 1926; Williams, 1932; Stoiber and Rose, 1969, 1970; Rose et al., 1970, 1976; Rose, 1972b, 1973a,b, 1987b; Smithsonian Institution, 1980–present; Anderson et al., 1995; Andres and Rose, 1995; Harris et al., 2002, 2003, 2004; Bluth and Rose, 2004; Sahetapy-Engel et al., 2004, 2008; Sahetapy-Engel and Harris, 2008; Forbes, 2010; Sanderson et al., 2010; Brill, 2011; Holland et al., 2011; Ebmeier et al., 2012) providing a first order basis for the detailed textural and morphological analysis of lava dome emplacement attempted

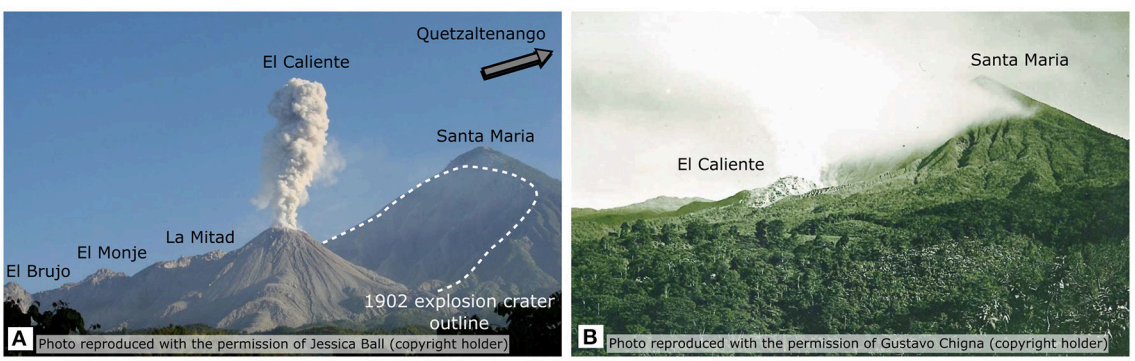

FIGURE 1 | (A) Photo of Santiaguito and Santa Maria from the south, showing a typical eruption from El Caliente. The four different domes are labeled. Quetzaltenango is Guatemala's second largest city and is located 10 km north. Photo from Jessica Ball. **(B)** Photo from a similar location in 1922, the first year of extrusion at El Caliente Dome inside the Santa Maria explosion crater. Photo source unknown, 1922.

herein. Extrusion cycles have been classified based on extrusion rate (Rose, 1973b; Harris et al., 2003), but as yet classification of lava types and how they fit into the eruption sequence has not been investigated. Thus, here we aim to classify lava types according to their texture and morphology, place them in within the eruptive sequence, and explain the origins of these textural variations and lava cycles.

GEOLOGICAL AND VOLCANOLOGICAL CONTEXT

Santa Maria is located on the southern edge of the Xela Caldera and is part of the Central American Volcanic Arc which extends from Mexico to El Salvador (**Figure 2**; Duffield et al., 1993; Bennati et al., 2011). Eruptive activity at Santa Maria began around 103 ka, and the edifice was constructed in four stages before a 25 thousand-year period of quiescence prior to 1902 (Rose et al., 1977; Rose, 1987a; Conway et al., 2013). Numerous lineations cut through the Santa Maria and Santiaguito edifices with a rough east to west orientation (**Figure 2**; Escobar-Wolf et al., 2010).

In 1902 Santa Maria underwent a devastating Plinian eruption, generating at least 8.5 km^3 dense rock equivalent (DRE) of dacite as ash- and pumice lapilli-fall deposits, and leaving an explosion crater or collapse scar on the southern base of the edifice (**Figures 1**, **2**; Rose, 1972a; Williams and Self, 1983; Singer et al., 2013; Andrews, 2014). After a period of quiescence of 20 years, volcanic activity resumed in 1922, with the extrusion of Caliente dome in the crater excavated in 1922 (**Figure 1B**). Volcanic activity has occurred without interruption, although at varying effusion rates. Thus far, four domes have been constructed—El Caliente (1922–1939; 1972–present day), La Mitad (1939–1949), El Monje (1949–1958), and El Brujo (1958–1986), extruding a combined total of ∼1 km^3 of magma (Harris et al., 2003). Following dome growth at El Caliente, La Mitad, El Monje, and El Brujo grew sequentially, moving progressively to the west until activity renewed at El Caliente coincident with activity at El Brujo in 1972 (**Figure 1**; Harris et al., 2003). The growth of the domes has been described by Rose et al. (1970) and Rose (1972b, 1987b) and units mapped with respect to time by Escobar-Wolf et al. (2010). El Caliente has been termed the main vent as it remained active with intense fumarolic activity throughout growth of the lateral vents, and

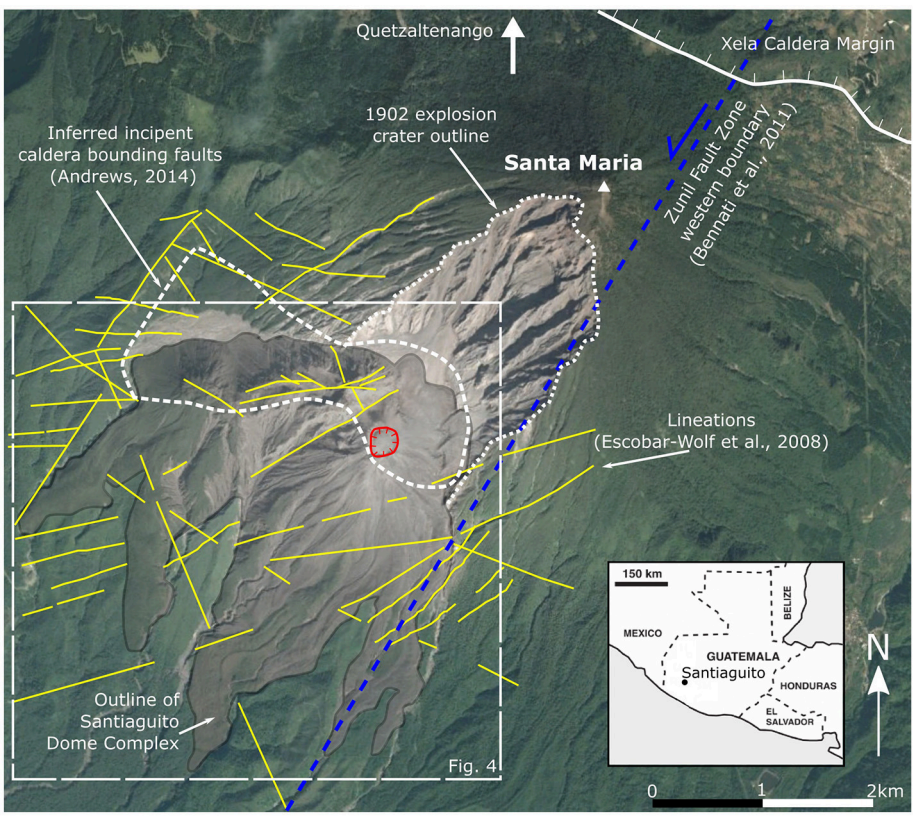

FIGURE 2 | Major structural features at Santa Maria and Santiaguito. Santa Maria lies to the south-east of the Xela Caldera Margin (84–12 Ma; Duffield et al., 1993), and sits on the western margin of the Zunil Fault Zone, both mapped by Bennati et al. (2011). The ∼1,000 m high erosional explosion crater and inferred incipient caldera bounding margin (Andrews, 2014) formed during the 1902 eruption are marked with a white dotted and dashed line, respectively. Lineations, defined by the alignment of topographic and or geomorphic features, possibly related to faults or joints, are displayed in yellow and were mapped by Escobar-Wolf et al. (2010). Santiaguito is shaded gray with the active El Caliente crater marked in red. Aerial photograph sourced from Google Map data ©2018.

has been the only center of activity since 1977 (Rose, 1972b, 1987b).

Cyclic Lava Extrusion

This study builds on and supports the view of Harris et al. (2003) that lava extrusion is cyclic, with 3–6 year-long episodes of high extrusion rate (0.5–2.1 m^3s^{-1}) followed by 3–11 year periods of low extrusion rate ($\leq$0.2 m^3s^{-1}). El Caliente is the most active dome at Santiaguito, experiencing multiple cycles of extrusion, at times coeval with activity at the other domes. Visual observations have documented multiple active vents at Caliente (e.g., April 1967: Rose, 1973b). To date, nine different cycles have occurred (Harris et al., 2003), with the latest emplacement of four lava flows >2 km in length in 2011–2015 signaling the start of a new cycle. [Note that during the writing of this study (late 2015 to early 2017), Santiaguito lava dome has experienced a period of heightened activity as explosions have lessened in frequency, increased in magnitude, and excavated a large crater inside El Caliente, before resuming a lava dome growth phase].

Activity prior to 1929 was endogenous, characterized by subsurface build-up of magma to inflate and uplift the carapace of the El Caliente dome. Between 1929 and 1958 a combination of endogenous and exogenous behavior occurred. Post 1958 growth has been solely exogenous, where lava extrudes at the surface (Rose, 1987b; Harris et al., 2003). In December 2012 (i.e., at the time of our field campaign), activity consisted of regular explosions ($\leq$2 h^{-1}) producing gas- and ash-plumes reaching heights of <1 km (Lavallée et al., 2015; De Angelis et al., 2016), and simultaneous lava flow extrusion accompanied by frequent incandescent rock falls. The recent observed behavior is consistent with activity at Santiaguito throughout its growth.

Lava Composition

The chemical composition of Santiaguito dome lavas has been thoroughly analyzed by Scott et al. (2012, 2013), as well as by Rose (1972b), Avard and Whittington (2012), and Singer et al. (2013). The first Santiaguito dome lavas extruded in 1922 were very similar to the 1902 eruption products: porphyritic dacites dominated by phenocrysts of plagioclase feldspar (~20–30%), and <5 % in total of pyroxene, titanomagnetite, and sometimes amphibole (Rose, 1972b; Singer et al., 2011; Scott et al., 2013). Although the phenocryst assemblage and abundance has not notably changed over time, the bulk SiO_2 content of erupted magma has become progressively less evolved with a decrease from 66 to 62 wt.% SiO_2 (Scott et al., 2013). Samples from Harris et al. (2003) indicated that this decrease happened gradually post 1970, but more recent research by Scott et al. (2013) suggest that the shift began as early as the 1930's and has been driven by magma mixing and fractional crystallization. Scott et al. (2012) suggest that the magma chamber developed in the lower crust, 12–24 km deep, with no evidence of a shallow storage zone. A stratified magma chamber model has been proposed with a vertical gradient in composition from a deep basaltic magma to a shallow dacitic magma. This model may explain the progressive depletion in silica content in eruptive products through time and the eruption of andesite at this stage (Scott et al., 2012).

Previous studies have highlighted that the various lava dome structures may be associated with distinct geochemical signatures (e.g., Rose, 1972b; Avard and Whittington, 2012). Most lava structures occur over the entire compositional range with a couple of exceptions. Spine structures only seem to have developed from dacitic lava with 64–66 wt.% SiO_2. Blocky lava flows that have reached distances exceeding 2.5 km from the vent seem to be characteristic of andesitic lavas with 62–64 wt.% SiO_2 (Rose, 1972b; Harris et al., 2003; Scott et al., 2012, 2013). Although there is a general trend associated with lava types and composition, various lava types and structures are observed within short periods of constant magmatic composition, and throughout the eruptive history at Santiaguito.

MATERIALS AND METHODS

Characterization

Mapping and sample collection at Santiaguito was carried out during a 4-week field campaign in November to December 2012. The outlines of units were based on high-resolution aerial orthophotographs taken in 2006 by the Instituto Geographico Nacional (IGN) of Guatemala. Features such as the outline of the main lava flows were adapted (in consultation with the authors) from Escobar-Wolf et al. (2010) and Ball et al. (2013). The focus of this study was on mapping summit features such as individual spines and lobes, their strikes and dips, and unique textural or structural features associated with them. Samples were taken from a range of these features on the dome summits and the recent lava flows, ranging in age from 1940 to 2012.

Porosity

The density and porosity of samples were measured by pycnometry of 25 mm diameter cylindrical samples using a Helium Ultrapycnometer 1000 at Massey University, New Zealand. We used dry rock equivalent densities of 2,616 $\pm$4 kg m^{-3} for summit dome samples, and 2,630 $\pm$4 kg m^{-3} for the 2012 lava flows (the closest spatially and temporally corresponding units from Avard and Whittington, 2012).

2D and 3D Textural Analysis

Textural analysis was undertaken to constrain the range of physical attributes of the lavas erupted. This was achieved quantitatively in 2D and 3D using a combination of techniques. Thin sections were prepared from rocks impregnated with epoxy containing a fluorescent dye, which eased the observation and delineation of pore space in UV light source. Complementarily, the crystal fraction was imaged under plane polarized light (PPL). A combination of manual tracing and ImageJ processing were used to threshold out and calculate the phenocryst crystallinity. Microlite crystal content required further analysis and 3–4 mm samples were prepared for backscatter imagery at the Scanning Electron Microscope (SEM) at the University of Canterbury. The microlites were traced out in Inkscape and quantified using ImageJ.

3D microtomography reconstructions aided with the interpretation of pore shapes from the flourescent thin sections and visually displayed their connectivity. Cross-sectional images

of 10-mm diameter samples were obtained using the Imaging and Medical beamline (IMBL) at the Australian Synchrotron in Clayton, Victoria and reconstructed and analyzed as 3D-image stacks in ImageJ. The scan energy of the beam was changed from 30 to 45 KeV as the samples varied in density. Pixel sizes of 2D images were either 6.10 or 13.73 μm, equivalent to voxel sizes in reconstructed 3D stacks of 227 and 2,588 μm^3.

Timing

The timing and interpretation of events was constructed from an exhaustive review of the literature and was aided by bulletins and photographs from: Smithsonian Institution Scientific Event Alert Network (SEAN) bulletins, Santiaguito Volcano Observatory (OVSAN) photographs, Instituto Nacional de Sismología, Vulcanología, Meteorología e Hidrología (INSIVUMEH) volcanic alert bulletins and NASA Landsat images. Photos and information from visiting and local scientists and observers also contributed (Bill Rose, Jessica Ball, Kyle Brill, Rüdiger Escobar-Wolf, Julio Cornejo).

RESULTS

Lava Type Characterization

Our historical summary, fieldwork, and textural analysis divide the lava types at Santiaguito into three main types: vesicular lava flows, blocky lava flows, and spines. Crystallinity (percentage of phenocrysts and microlites) are consistent between the lava types (**Table 1**). Typically lava domes with high crystallinities have pore shapes controlled by crystals, producing irregularly shaped pores with ragged pore walls reflecting the inward protrusion of crystals (microlites and phenocrysts; Hammer et al., 2000; Kendrick et al., 2013). This is also the case for the Santiaguito lavas. Despite this, a significant range of porosity and pore textures are exhibited and we use these in combination with morphology to characterize the lava types.

Here, we present the morphology (**Figure 3**) and distribution (**Figure 4**), bubble and crystal textures (**Figures 5–7**) and relationships between the lava types (**Figure 8**). A summary of results is provided in **Table 1**.

Vesicular Lava Flows

These refer to lava flows with coherent, vesicular (a'a-like, yet unbrecciated) flow top and a steep rounded front (**Figure 3**). [Note that this is not easily classified by existing lava flow morphology nomenclature, i.e., it is not a'a or blocky, thus we are limited to the use of "vesicular lava" in this study] Vesicular lava flows are restricted to the summit zone of the domes (**Figure 4**). An example of vesicular lava was witnessed extruding from El Caliente after moderate dome and summit lava flow collapse on November 28th 2012 (this field expedition; **Figure 3A**). In most cases vesicular lava flows are overprinted by subsequent eruptions and not preserved (i.e., the November 2012 flow was overprinted by unit Rcs). The units Rbe (erupted in 1978) and the beginning of Rma (erupted in the 1950's) are examples of vesicular lava flows (**Figure 4**). There are numerous historical accounts and photographs of vesicular lava at Santiaguito, most notably following the explosion and dome collapse in 1929, and when activity returned to El Caliente in 1972 (Anderson et al., 1995).

In our samples of vesicular lava from El Brujo (flow top and interior) porosity is high, ranging from 35 to 70% (**Figure 5**). The pores are spheroidal and interconnected, with dominantly convex edges and with concave remnant pore wall protrusions (**Figure 6**). In thin section, pores reach a maximum diameter of 10 mm in size, however tomography (**Figure 6**) and connected porosity data (**Figure 5**) show that these pores form a connected network reaching total lengths of several centimeters and extending beyond the dimensions of our 40-mm samples. Pores from the top of the flow are not strongly

TABLE 1 | Summary of lava properties by type.

	Vesicular summit lava flow	Blocky lava flow	Spine
Description	Short very vesicular flow with a rounded coherent top	Short to long lava flow with mixed porosity and a blocky top	Dense sub-vertically extruded units
Rough Volume	Low (<300,000 m^3)	Low—High (200,000–1,600,000 m^3)	Low (<400,000 m^3)
Dip	Low (5–30°) with steep dipping flow fronts (>50°)	Low (5–30°) with shallow (32°C)[ɤ] to steep (70°) dipping flow fronts	High (38–90°)
Porosity (range)	35–70%	3[†]−79%	4–23%
Pore Textures	Round, interconnected pores	Zones of larger round and smaller tubular interconnected pores with evidence of flattening and stretching	Small skeletal interconnected pores (primary) and dilational pores with ragged pore walls (minor)
Crystallinity	31–34%	30–35%	27–34%
Microlites (% of groundmass)	37–40%	40–43%	41–45%
Composition	62–65 wt.% SiO_2	62–65 wt.% SiO_2. Note blocky lava flows that exceed distances of 2.5 km from the vent have a more limited SiO_2 range of 62–64 wt.%	64–65 wt.% SiO_2
Extrusion Rate	High	Low–High (0.2–2.1 m^3s^{-1})	Low (≤0.2 m^3s^{-1})

[†] *Avard and Whittington, 2012.*
[ɤ] *Harris et al., 2006.*

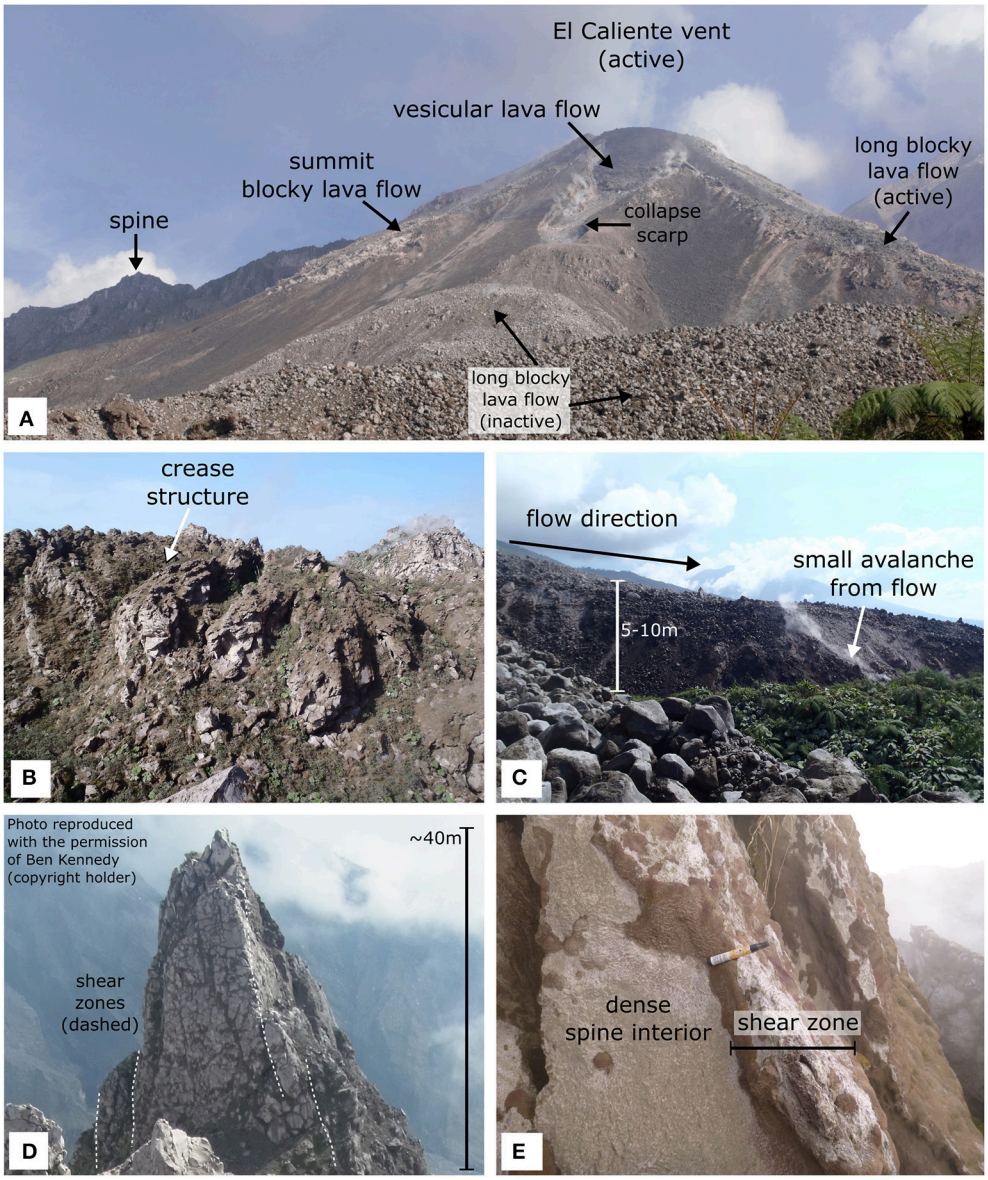

FIGURE 3 | Photos of lava types. **(A)** El Caliente from the south, November 2012, where a vesicular lava is infilling a recent collapse scarp, and long blocky lava flow and summit blocky lava flow are also active. Spines from El Monje can be seen in the distance. **(B)** A vesicular lava flow on El Brujo, this flow is semi-circle shaped and exhibits a crevasse with features similar to crease structures described at Mount St. Helens by Anderson and Fink (1992). **(C)** A long blocky lava flow ~1 km from the vent. **(D)** A prominent spine on La Mitad. **(E)** Close up of a spine showing the dense spine interior and shear zone rim.

aligned, though thicker horizontal bands of coalesced pores are present.

Blocky Lava Flows

Blocky lava flows generally have a coherent interior, and a top surface composed of smooth sided, angular–subrounded blocks 0.1–2 m in size (**Figure 3**). Blocky lava flows extrude from low points in the active dome, however their thickness causes their upper surface to be ~10 m above the vent rim. The flows reach 70 m thick, 500 m wide, and vary in length from 400 m to 4 km (**Figure 4**). These flows follow local depressions, typically river channels. Blocky lava flows vary significantly in volume and have been divided up by length into summit blocky flows and long blocky flows for some of our results (**Figures 4**, **8**).

Summit blocky lava flows are low-volume flows, which extend a short distance down the sides of the dome, but never reach the base. The units Rbf and Rbh (erupted in 1975) are examples of summit blocky lava flows (**Figure 4**). These flows repeatedly collapse at the flow toe due to their low volume and the high slope angle ($\geq 35^{\circ}$) from the eruptive summit to the flank of the dome, producing block and ash flows. This collapse dynamic may have prevented the flow front from reaching the base of the dome.

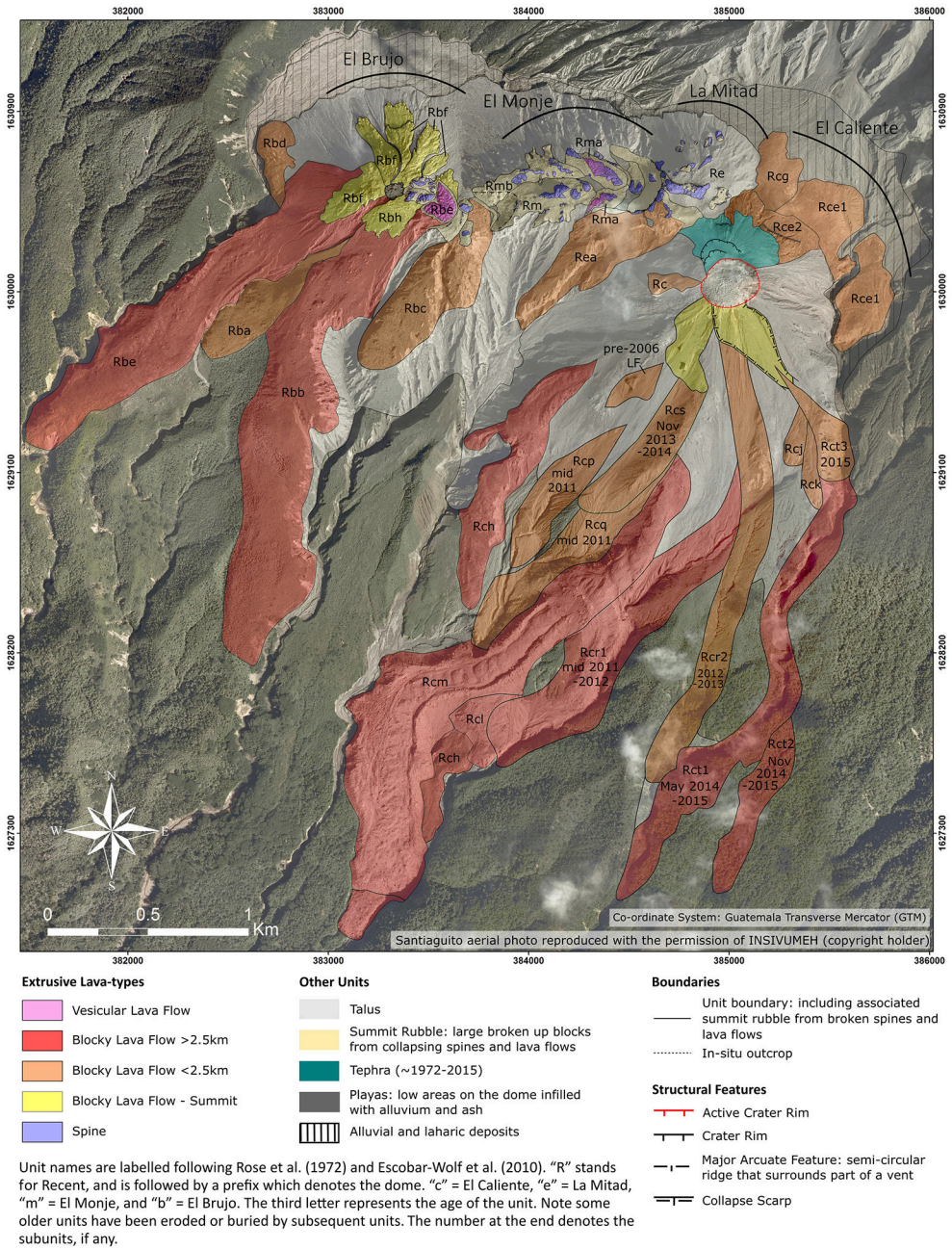

FIGURE 4 | Lava type map of the Santiaguito Lava Dome Complex. This map is developed as a companion map to Escobar-Wolf et al. (2010) and Ball et al. (2013). Pre–2010 dome and lava flow features were mapped by Escobar-Wolf et al. (2010) and Ball et al. (2013) from aerial 0.5 m pixel resolution aerial orthophotos 1860-II-14 and 1860-II-19 (acquired between November 2005 and April 2006 by the Instituto Geográfico Nacional) as well as by direct field mapping. Recent post–2011 collapses and lava flows were mapped from NASA ASTER images, field observations, INSIVUMEH photos, and Google Earth.

Long blocky lava flows are the highest volume end member, and largest volume extrusive products at Santiaguito. The units Rbb (erupted in 1959–1963) and Rcm (erupted in 2001–2004) are examples of long blocky lava flows (**Figure 4**). A single long blocky lava flow may continue growing for a few years and as a result these flows have the most pronounced ogives (pressure ridges) and levees (**Figures 3**, **4**). Regular small block and ash flows and avalanches (>1 min^{-1}, reaching up to 400 m) initiate from collapse of both the flow front and sides. Flow fronts of long flows may collapse to form block and ash flows reaching kilometers from the flow front such as in 1976 (Rose et al., 1976).

Vesicularity is heterogeneous, at both outcrop scale and micro scale. The top 5–10 m of long blocky lava flows are more vesicular

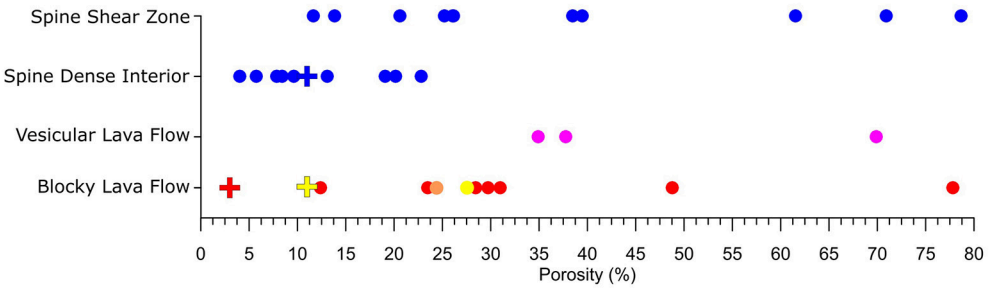

FIGURE 5 | Total porosity of extrusive products at Santiaguito. Circles are data from this study, and crosses are values from Avard and Whittington (2012). Blocky lava flows are separated into: summit blocky flows (yellow), blocky lava flows that reach the base of the cone but do not extend further than 2.5 km length (orange), and blocky lava flows >2.5 km (red). Less than 1% of the porosity was isolated in all the samples used in this study, so only total porosity is shown, equivalent to the connected porosity.

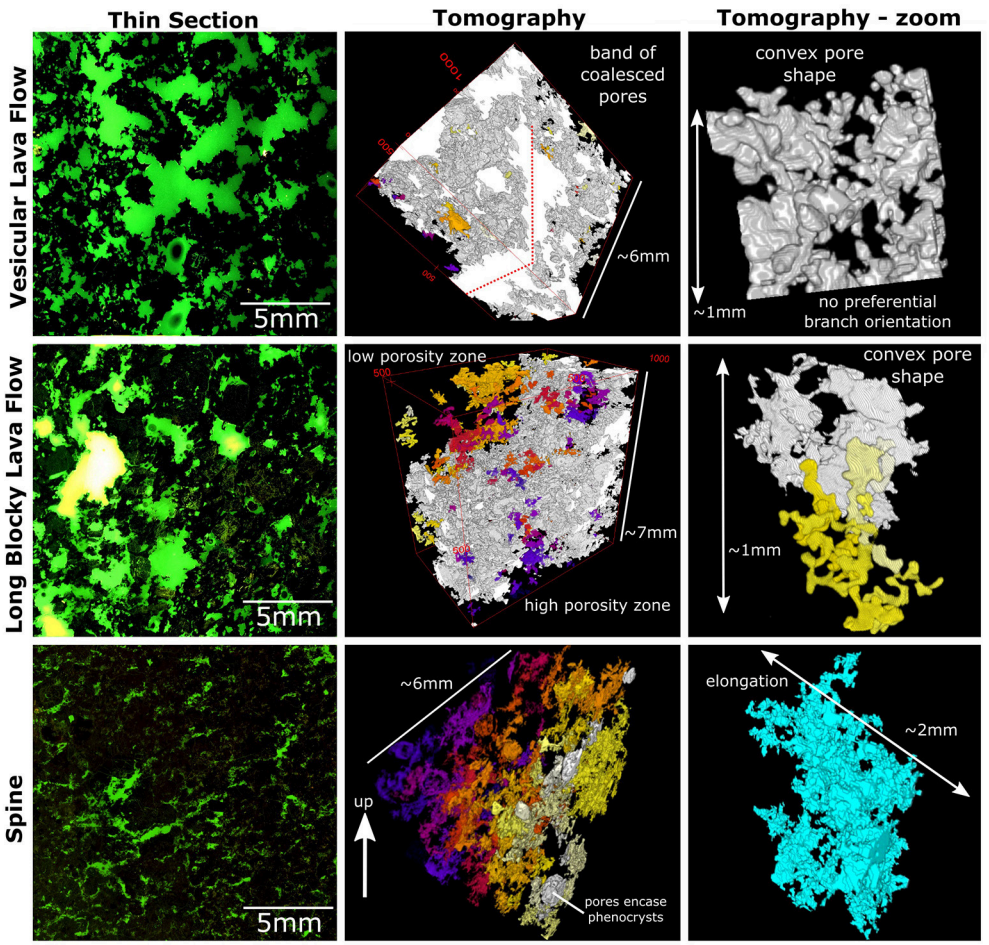

FIGURE 6 | Ultra-violet pictomicrographs and tomography imaging of pores in vesicular and blocky lava flows, and of the dense interior of spines. Different colors in tomography images represent connected pores, and the 100 largest pores are displayed in the images.

than the bulk of the interior as seen on La Mitad (this study) and on El Brujo (Rose, 1972b). This vesicularity difference is reflected in the samples from the blocky top (3–79%; **Figure 5**). Pores range in shape and size between and within samples, including larger round pores as seen in vesicular lava flows, and slim tube shaped interconnected pores with varying degrees of flattening and shearing that are unique to blocky lava flows (**Figure 6**).

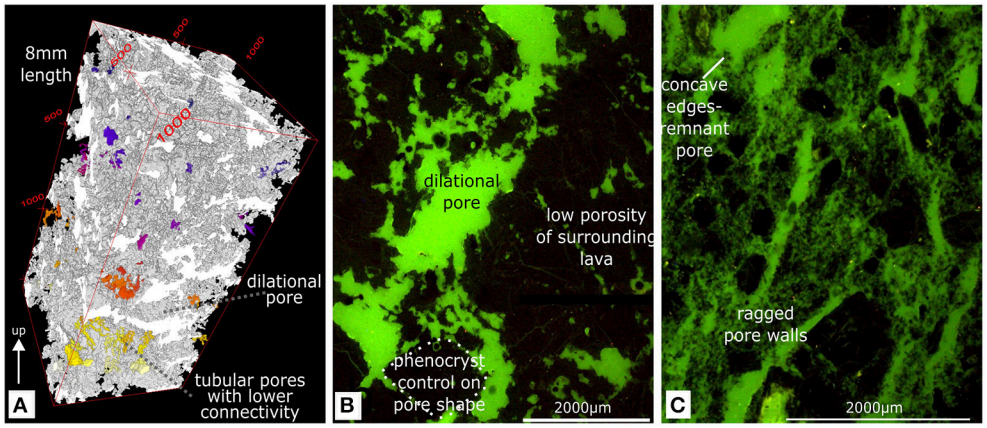

FIGURE 7 | (A) Tomography of pores in a vesicular zone bordering a spine. The 100 largest pores are displayed in the image in different colors. Note the high connectivity of dilational pores (white) and zone of lower porosity with lower connectivity (bottom corner). **(B)** UV photo of flow band in a spine showing interconnected dilational pores and phenocryst control on pore shape. Most pore walls are concave and convex in this example. **(C)** UV photo of a shear zone with ragged pore walls marked by the protrusion of groundmass fragments and phenocrysts. Remnant concave pore walls of previous pores are also visible. Note subvertical alignment of pores.

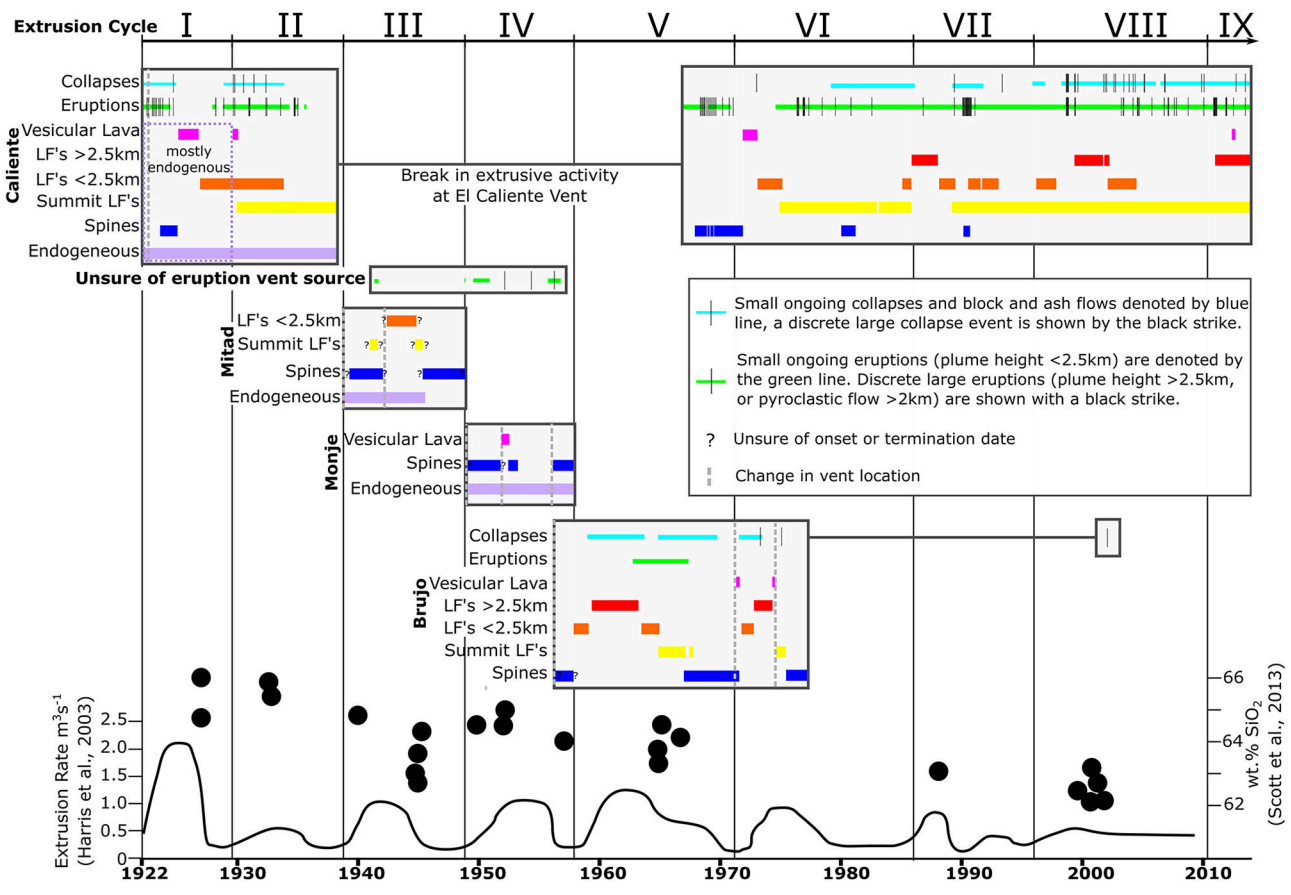

FIGURE 8 | Timing of extrusive activity and eruptive and collapse events at Santiaguito with reference to extrusion cycles (Harris et al., 2003), composition (Scott et al., 2013), and extrusion rate (Rose, 1973b; Harris et al., 2003).

As with vesicular lava flows, in thin section pores reach a maximum diameter of 10 mm; however tomography and connected porosity show that these pores form connected networks reaching total lengths of several centimeters and extending beyond the dimensions of our 40-mm samples (**Figures 5**, **6**). Pores in the samples with the highest porosity have dominantly convex pore surfaces with concave remnants of bubble-wall protrusions, which indicate pore coalescence and/or collapse by shearing. These convex pores are the lar4gest pores in blocky lava flows and are usually connected to other large pores. Many of these interconnected pores show preferential long-axis alignment, and are more aligned than the vesicular lava flow pores.

In the densest samples the pores have smaller maximum diameters. Some pores have both concave and convex surfaces and evidence of remnant pore-wall protrusions, but have little alignment, which are similar to some pores seen in spines. However, in most cases this pore morphology is aligned, with dominantly convex pore walls and little evidence of pore-wall protrusions. These pores form networks of interconnected tubes, and are unique to blocky lava flows. All pore types are dominantly located adjacent to phenocrysts and lithic inclusions (**Figure 6**). Blocky lava flows can be preceded or followed by spine extrusion.

Spines

Spines are dense, coherent masses of lava that extrude subvertically above the vent along linear fault-controlled planes (**Figure 3**). They are low volume, and limited to the summit zone of the domes. The largest spines reach 200 m long, 50 m wide, and 70 m tall and the smallest spines are only 3 × 5 m (**Figure 4**). The spines exposed on the domes today are commonly characterized by zones of fractured dense material (>3 m wide), separated by regularly spaced subvertical scoriaceous or brecciated zones (<1 m, here termed "shear zones"; **Figure 3**). Observations of spine extrusion at Santiaguito report that sections of spines regularly collapse forming block and ash flows that reach the base of the dome, or are repeatedly disrupted by explosive events (Williams, 1932; Rose, 1973b).

Most spines appear to have extruded near-vertically, whereas a few spines have curvilinear surfaces that appear drooped and folded exhibiting some features similar to whaleback structures at Montserrat described by Watts et al. (2002). The difference between these low angle spines and the lava flows is that they are much denser and have shear zones on the outer edges. Similar features have been described at Unzen volcano (Smith et al., 2001; Hornby et al., 2015), Soufrière Hills (Watts et al., 2002), and Mount St. Helens (Gaunt et al., 2014; Kendrick et al., 2014).

The largest of the exposed spines form the prominent ridges on La Mitad and El Monje domes [units Re (erupted in 1931) and Rm (erupted in 1950); **Figure 4**]. These spines tend to have multiple widely spaced shear zones marked by more vesicular rinds at the edge of each dense core (**Figure 3**). Commonly a vertical gap is observed in the center of, and parallel to, a shear zone. The gaps widen toward the top of the spine, implying that the denser sections of the spines may have moved apart laterally at the weaker shear zones during extrusion. On a larger scale the major shear zones interweave. Note that shear zones are distinct from cooling joints, which are not marked by a change of texture or vesicularity.

The inside of the spines are dense, but the outside surface may either be smooth, or have a thin brecciated or vesicular rind—"shear zones" (**Figure 3**). The dense zones within the spines have low porosity (4–22%; **Figure 5**), and the pores are similar in shape and size between samples. In thin section the pores reach a maximum of 5 mm in diameter; however tomography and connected porosity data show that the pores form large interconnected networks within the 40-mm sample size.

The most common pore type is very thin, skeletal-shaped interconnected pores (**Figure 6**). These have both convex and concave pore surfaces, evidence of remnant bubble-wall protrusion, and the largest examples always border phenocrysts. Tomography shows that these pores form skeletal-like networks of interconnected pores that are aligned extrusion-parallel in our samples. In contrast to the thin tubular pores in the lava flows, the pore networks predominantly align in thin, tightly spaced vertical planes, with lesser lateral connectivity than vertical. Occasional convex surfaces, bulbous pores, and pore-wall remnants characteristic of more round interconnected pores are observed within the porous network.

Shear zones within the spines generally have a higher porosity (11–79%) than the dense spine interior (4–22%; **Figure 5**) and are texturally variable. The shear zones can broadly be differentiated into two end members: vesicular and brecciated. Tomography and thin-section show that the vesicular samples have an en-echelon pattern of interconnected sigmoidal pores (**Figure 7**). The sigmoidal pores have convex and concave pore surfaces. Pores may be large and widely spaced or thin and closely spaced and the largest examples always border phenocrysts and have evidence of remnant bubble-wall protrusion.

In thin section the shear zone pores reach a maximum of 10 mm in diameter; however tomography and connected porosity data show that the pores form interconnected networks within the 40-mm sample size (**Figures 5**, **7**). Small sigmoidal interconnected pores also form along flow bands within the dense spine interior. In thin section the dense interior shows local en-echelon bands with remnants of previous rounded or thin interconnected pores. The length of the chain often extends beyond the length of the 40 mm thin sections and thus cannot account for the full scale of the feature observed in the field. Yet, the geometrical relationship observed in the micro- as well as the macro-textures, such as S-C fabrics (showing the intersection of S-planes oblique to shear surface and C-planes parallel to shear surface), sigmoidal pores and crystal alignments suggest simple shear in these regions of strain localization.

The brecciated shear zones host the dense rocks from the spine interior. We note that the porosity increases slightly and the crystal size decreases along the edge of the spine. The clasts in the shear zones are generally highly brecciated at the macro-scale (clasts 1–30 mm in size) and partially fragmented internally at the microscopic scale. This may be analogous to the cataclasite zones described at Mount St. Helens (Pallister et al., 2012) and have similar properties to those described in the 1994–1995 spine erupted at Unzen (e.g., Smith et al., 2001).

Timing of Lava Types at Santiaguito

The characterization of lava types allowed a re-examination of the timing and progression of lava types at Santiaguito. This synthesis of data is presented in **Figure 7**, with an accompanying map of all the currently exposed extrusive products in **Figure 4**. The timeline builds on and supports Harris et al. (2003) view that lava extrusion is cyclic.

A typical eruption cycle begins with an increase in extrusion rate and the early extrusion of spines, often from a new vent. Spine growth is generally preceded by or coincident with endogenous growth as the extrusion rate was low but steadily increasing. As the extrusion rate increases, lava flows of increasing length are emplaced. Toward the end of a cycle the extrusion rate declines again, and the trend is reversed culminating in spine growth. The next phase of activity typically resumes at a new location.

Over time the lava type end members in the cycles changed. Prior to 1980, alternation between spine formation and blocky lava flows of moderate lengths dominated the eruptive sequence. Since 1980, blocky lava flows of variable lengths were erupted from the summit of Caliente dome. Blocky lava flows in excess of 2.5 km in length were not extruded prior to 1965 and have become increasingly dominant since. This transition has coincided with the less frequent spines, becoming significantly smaller in size and volume, and no spines have been extruded since 1990.

Infrequent larger eruptions and dome or lava flow collapse events have caused larger ash plumes (<6 km) and block and ash flows (Rose, 1973a; Rose et al., 1976; Fink and Kieffer, 1993). The most notable of which occurred in 1929 when a collapse and explosion at El Caliente sent a pyroclastic density current 11 km downstream, killing ∼5,000 inhabitants in the town of El Palmar (Rose et al., 1976; Simkin et al., 1994). Vesicular lava often follows collapse events.

The timeline highlights how lava types correspond with and respond to the extrusion rate and eruption history, including the effects of slope, cooling, degassing, and crystallization during emplacement.

DISCUSSION

Controls on Lava Dome Morphology

This review, synthesis and new data concerning timing of lava types has revealed remarkable cycles in lava extrusion style. Lava domes may extrude varying lava styles, from endogenous lobes to exogenous lobes or spines (e.g., Manley, 1996; Fink and Griffiths, 1998; MacKay et al., 1998; Nakada et al., 1999; Harris et al., 2002, 2004; Navarro-Ochoa et al., 2002). The development of varying lava styles depends on lava viscosity and extrusion rate (Anderson and Fink, 1989; Swanson and Holcomb, 1990; Watts et al., 2002; Zobin et al., 2002; Pallister et al., 2012), which dictates the development of the shear zones that control extrusion dynamics (e.g., Lavallée et al., 2007, 2013; Tuffen et al., 2013; Kendrick et al., 2014). We attribute the changes in morphology to (1) an evolving source composition and temperature decrease over time (Scott et al., 2013), and (2) conduit processes such as degassing, outgassing, and strain rate driven viscosity changes and the evidence for this is preserved in the pore shapes and sizes.

Several variables have been suggested to control the viscosity of dome lavas; principally melt composition and temperature (Giordano et al., 2008; Mueller et al., 2009) as well as crystallinity (Caricchi et al., 2007), porosity (Caricchi et al., 2011), and strain rate (Lavallée et al., 2007, 2013; Cordonnier et al., 2009; Kendrick et al., 2013).

Consistent with the bulk rock composition, interstitial glass analyses of Santiaguito lavas display a large range in composition (rhyolite–trachyte–dacite), broadly decreasing in SiO_2 with time, although the SiO_2 content of the glass in individual samples

TABLE 2 | Temperatures at Santiaguito.

References	Temperature	Extrusive unit and method	Eruptive/Pre-eruptive temperature
Andrews, 2014	840–850°C	Phase equlibria experiments of natural pumice and phenocryst compositions of the 1902 Santa Maria dacite.	Pre-eruptive (Santa Maria)
Singer et al., 2013	870°C	Fe-Ti oxide + two pyroxene geothermometry and melt inclusion compositions.	Pre-eruptive (Santa Maria)
Scott et al., 2013	900–1,000°C	Phenocrysts from Santa Maria pumice using the thermobarometer of Ridolfi et al. (2010).	Pre-eruptive (Santa Maria)
Scott et al., 2012	940–980°C (±20°C)	Matches amphibole rim widths and best represents geochemistry conditions at Santiaguito over its history.	Pre-eruptive (Santiaguito)
Sahetapy-Engel et al., 2004	850–950°C	Maximum temperatures calculated at the surface of the El Caliente vent in 2002 using an infrared thermometer, spectroradiometer and digital video camera.	Eruptive at vent (Andesite, high eruption rate and extrusion of 4 km blocky lava flow)
Harris et al., 2002, 2003	496–531°C	Highest direct measurements taken of the 1999–2002 (Rcm) flow front core 2.5 km from vent. Note: used eruption temperatures 833°C from Scaillet et al. (1998) for thermal modeling.	Eruptive at the flow front (Andesite, high eruption rate and extrusion of 4 km blocky lava flow)
Scaillet et al., 1998	833°C (800–850°C)	Fe-Ti oxide geothermometry on the Santa Maria pumice. Used method from Ghiorso and Sack (1991).	Pre-eruptive (Santa Maria)

(within a given eruptive unit) may range by up to 10 wt.% (Scott et al., 2012). Along with the composition, the temperature of the reservoir feeding Santiaguito has likely increased (**Table 2**). The early Santiaguito lavas were very similar to the 1902 eruption products (Rose, 1972b; Singer et al., 2011; Scott et al., 2013) and may represent a pocket of left-over dacite in the magma reservoir (e.g., Scott et al., 2013; Singer et al., 2013); thus we assume that they erupted at a temperature similar to the Santa Maria eruption of around 850°C (Scaillet et al., 1998; Singer et al., 2013; Andrews, 2014). Over time as progressively more andesitic magma was erupted we expect that the temperature of the magma increased, to reach a maximum of 950°C, as estimated by Sahetapy-Engel et al. (2004), and supported by Scott et al. (2013) based on amphibole geothermometry. Similarly, there have been <8% changes in crystal fractions and Scott et al. (2012) hypothesized that crystallization may be limited at shallow depths due to a "final quench" where microlites stop nucleating and growing.

To a certain extent, magma chamber stratification and resultant shift in composition and temperature has influenced the lava structures and extrusion cycles over time. In particular spines only formed when dacitic lava was extruded and flows extending over 2.5 km only formed in andesitic lavas. However, various lava types and structures are observed within short periods of similar and arguably relatively constant pre-eruptive composition, temperature and crystallinity, and indicate that the pre-eruptive conditions (i.e., the physico-chemical state in the reservoir before ascent) are not the only control on lava morphology.

Our evidence suggests that in addition to composition, conduit processes such as degassing, pore configurations, strain rate, and thermal shifts during ascent also drive the viscosity changes responsible for the variations in dome eruption style at Santiaguito. The relatively open magmatic system (Bluth and Rose, 2004; Holland et al., 2011) and the slow magma ascent likely allowed for efficient outgassing through the interconnected porous network, which is observed in all lava types (**Figure 6**), and obvious from continuous gas emission observations at Santiaguito. The amount of dissolved water in the melt during extrusion is unknown at Santiaguito owing to a number of challenging issues arising in these dome lavas. As such, here, we turn to pore textures as evidence of degassing and outgassing and a schematic model of pore development is presented in **Figure 9**.

We attribute the observed differences in pore shapes and volume to be initially reflecting shallow inflation, deflation, and coalescence of the exsolved bubble volume. Inflated interconnected pores such as in vesicular lava flows and high porosity zones of blocky lava flows show complex pore shapes and remnant pore wall protrusions from coalescence. In deflated interconnected pores such as in spines and dense zones of blocky lava flows, the remnant pore-wall protrusions are smoothed as decreasing gas pressure due to outgassing allows surface-tension-driven deformation (e.g., Kennedy et al., 2016). Inflated pores likely indicate a lower viscosity and perhaps a residual water content in the vesicular and blocky lavas.

Pores may have additionally undergone a degree of flattening and stretching, indicating preferential compaction or shear

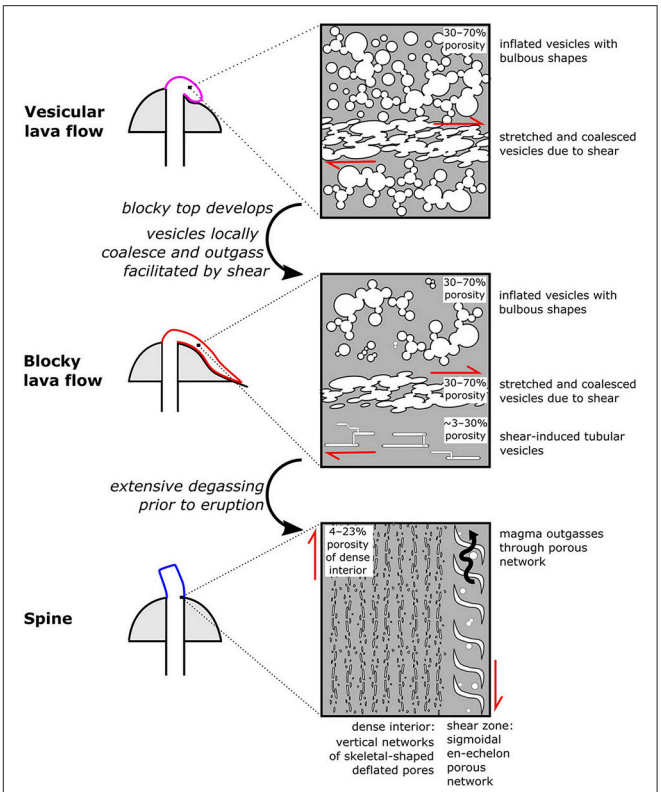

FIGURE 9 | Conceptual model of pore development at Santiaguito.

(Rust et al., 2003; Wright et al., 2006; Kendrick et al., 2013; Ashwell et al., 2015). Stretching of deflated pores results in a network of tube-shaped pores with a preferential alignment in lava flows, or skeletal-shaped pore networks that are aligned along "extrusion-parallel" planes developed in spines (**Figure 6**). Stretching of inflated pores produces sheet-like pores that form flow bands in the lavas. Shear can additionally facilitate outgassing and deflation by increasing the connectivity between pores (e.g., Okumura et al., 2009; Caricchi et al., 2011). This was shown experimentally on Santiaguito samples by Avard and Whittington (2012) at strain rates representative of long blocky lava flows, and is observed in our dense zones of blocky lava flow samples (**Figure 6**).

A distinct form of flow bands with en-echelon sigmoidal pores form along spine margins (**Figure 7**). These are characteristic of dilation where brittle failure of magma results in tension gashes that rotate into sigmoidal shapes and are influenced by phenocryst and remnant pore location (Kendrick et al., 2012; Lavallée et al., 2013). The ragged pore walls in places indicate the magma was torn slowly (unlike straight failure planes produced at high shear rates; see Lavallée et al., 2013). Such tearing structures have also been observed at Unzen, Yakedake, and Daisen by Smith et al. (2001). The high porosity and connectivity of these shear zones likely contribute to outgassing. The considerable evidence of pore collapse in the dense core of spines, bordered by elongate, shear-driven porous bands

in these lavas suggest efficient outgassing during ascent and extrusion.

Advances to the Understanding of Cyclic Lava Extrusion at Santiaguito

Here we incorporate our observations and textural analysis with previously published models to build on the growing understanding of cyclic lava extrusion at Santiaguito. The textures and eruption history support a model of a gradually changing reservoir composition and temperature, which is modified by conduit outgassing and localized shear, to dramatically change the viscosity and eruption style of the lava. The timing of the lava types illustrated in **Figure 8** highlights how lava types correspond with and respond to the extrusion rate and extrusion history documented by others.

At Santiaguito, extrusion rate is cyclical with 3–6 year-long phases of high extrusion rate (0.5–2.1 m^3 s^{-1}), followed by a longer (3–11 year) phase of low extrusion rate (0.2 m^3 s^{-1}; Harris et al., 2003). Extrusion rate determines the time in the shallow conduit available for (1) outgassing, reflected in the pore volume and structures, and (2) cooling, influencing viscosity. Lavas at Santiaguito have a viscosity measured to range between $\sim 10^9$ and 10^{12} Pa.s (Harris et al., 2002; Avard and Whittington, 2012), with spine structures likely on the upper end of this, as at other domes worldwide spines are generally lower temperature and higher viscosity than flows (Nakada and Motomura, 1999; Schneider and Vallance, 2008; Cordonnier et al., 2009). The lava types reveal a progression from porous short flows with inflated pores and coherent flow tops through long lava flows with varied pore morphology and blocky flow tops to spines with deflated pores and well developed porous shear bands. A model for lava type progression is presented in **Figure 10**.

Activity at Caliente, Mitad and Monje all commenced with endogenous growth (**Figure 10**). Although we do not have good time constraints of endogenous growth it probably accompanied all lava types prior to 1958, and we refer to this phase as "leaky" endogenous. Growth at El Caliente was mostly endogenous until the second extrusion cycle began in 1929 (Harris et al., 2003).

Perhaps the most notable event in extrusion cycle II was the November 1929 dome collapse, as the extrusion rate was increasing at El Caliente. The collapse was followed by the extrusion of vesicular lava.

The most porous lava type, vesicular lava, is extruded after large eruptions or dome collapses (**Figure 10**). The clearing of overlying, more-degassed lava allows fresh magma to ascend relatively quickly, without significant degassing; as a result the lavas vesiculate late at (or near) the surface forming spheroidal vesicles. The vesicular lava flow extrusions coincide with less regular gas explosions, e.g., after the November 2012 collapse. Upon continued extrusion and flow, the flow top of the initially summit-limited, vesicular lava (**Figure 11A**) apparently evolves in time and space into blocky lava (**Figure 11B**). Simultaneously in the flow core of the blocky lavas, vesicles progressively collapse and outgas during shearing and flow advancement. In **Figure 11C**, we show that other proximal lavas exhibit a moderate degree of flow-top brecciation as they spill from a collapse scar with a surface morphology intermediate between the coherent flow tops of the vesicular lavas and the blocky lavas.

Blocky lava flows extrude at high and low extrusion rates and have a connected network of inflated and deflated pores. The longest lava flows were emplaced during constant, high-extrusion rates that can last up to 2 years (**Figure 8**; Harris et al., 2003). Eruptions and fumarolic activity occur simultaneously with long blocky lava flow extrusion (Rose, 1973a; Bluth and Rose, 2004; Johnson, 2004; Brill, 2011; Holland et al., 2011) indicating outgassing in conduit. Outgassing continues as the lava flows downslope. This is evidenced by further vesicle reconfiguration, localized shear flattening, stretching and deflation (e.g., Manley and Fink, 1987; Avard and Whittington, 2012; Ashwell et al., 2015; Kennedy et al., 2016) in the flow core. Gas percolates through the permeable network locally creating layers of highly vesicular lava immediately below the dense blocky top. These spatially heterogeneous processes are reflected in the spatial heterogeneity of porosities (vesicles and fractures) in the flows. At any time during flow, lava may be quenched at the flow front or edges, preserving a complex history of pore inflation, deflation, and shear from different parts of the flow.

During periods of low extrusion rates, lava flows of decreasing length develop, and prior to 1990 the dacitic composition favored conditions suitable for spine growth (**Figure 8**). Spines precede and follow blocky lava flows and have dense interiors containing small, connected, deflated pore networks. Intermittent planar vesicular shear zones with en-echelon sigmoidal pores separate the dense interiors. The low extrusion rate allows time for prolonged degassing, outgassing (evidenced by pore deflation) and cooling in the conduit likely causing viscosity increases that may prompt spine extrusion (**Figure 10**). Extrusion is accompanied by mild steam eruptions (Williams, 1932; Rose, 1973b), likely initiated along the planar vesicular shear zones, further aiding outgassing.

The recent andesitic eruptive period (1990–2016) switches between the extrusion of vesicular and blocky lavas with length corresponding to extrusion rate, dome collapses, and eruptions. Hence the progressive change in the geochemistry of the erupted lavas in the last century from dacite to andesite (e.g., Scott et al., 2013) may have influenced the temporal occurrence of switches in eruptive activity.

CONCLUSIONS AND IMPLICATIONS

Our new mapping and textural data allowed us to categorize lava types at Santiaguito. Following this an extensive review of all lava types and timing was conducted to create a timeline of extrusive activity at Santiaguito.

(1) There are three main lava types at Santiaguito: vesicular lava flows, blocky lava flows, and spines. These types reveal a progression from porous short flows with inflated pores through to long lava flows with varied pore morphology to spines with deflated pores and well-developed porous shear

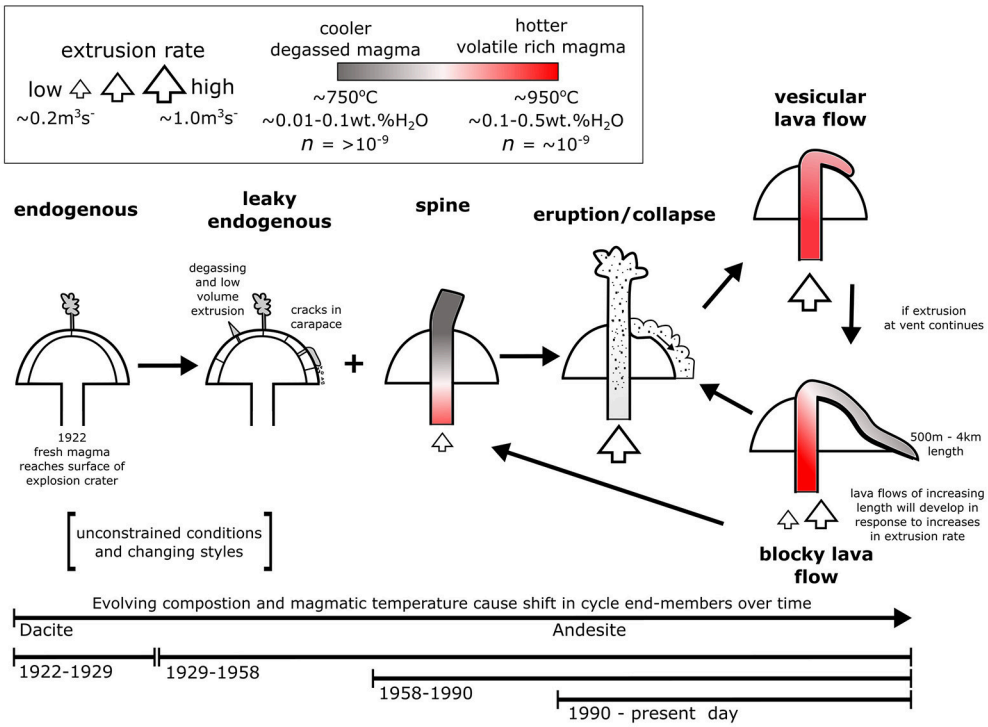

FIGURE 10 | Cyclical model of extrusive activity at Santiaguito.

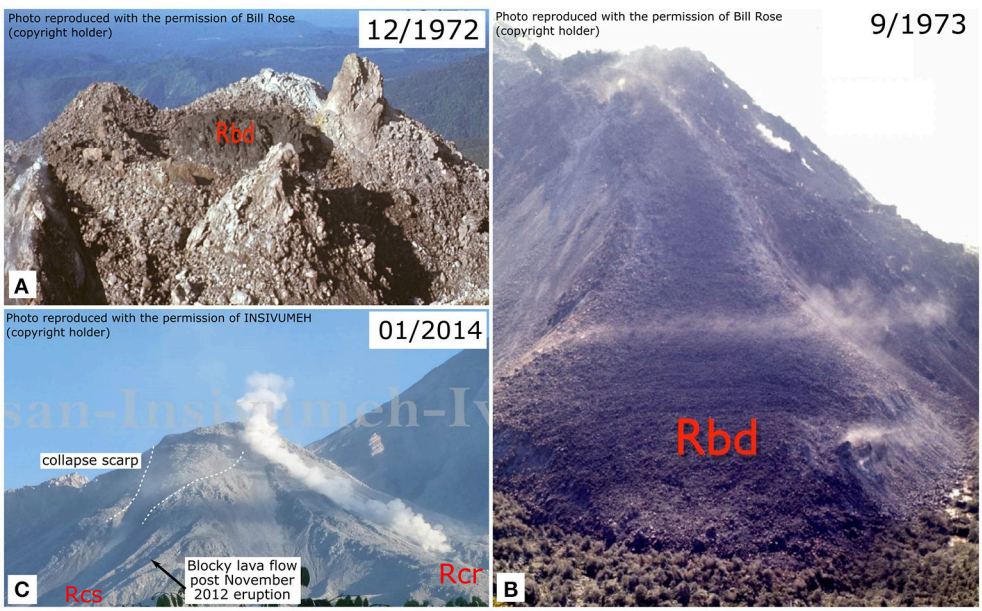

FIGURE 11 | Evolution of vesicular lava into blocky lava. **(A)** Vesicular lava extruding on El Brujo, surrounded by older spines. **(B)** Photo of the same flow front, 10 months later, with increased brecciation of the flow top. **(C)** Proximal lava infills a collapse scarp; the lava flow top is made up of large blocks in comparison to longer flows (as in **B**). See also the blocky lava flow (Rcs) that advanced in the months after the November 2012 collapse, following the initial vesicular lava flow. Note the small block and ash flow descending the dome.

bands. There is no significant differences in crystal content between these lava types.

(2) The timing of the lava types highlights how they may respond to the extrusion rate and extrusion history (including the effect of slope, cooling, and degassing). Blocky lava flows of increasing length develop at high extrusion rates and spines extrude at the beginning and end of an extrusion cycle at low extrusion rates. A collapse or eruption may cause a shift to extrusion of vesicular lava flows.

(3) Our new textural data when reviewed with all the other published data allows a model to be developed: The model demonstrates the importance of (1) initial magmatic composition and temperature, and (2) effusion-rate-driven degassing, outgassing, and cooling in the conduit, and hence viscosity, in controlling the eruption style and associated lava types.

Each lava type presents a unique set of hazards:

(1) Vesicular lava has the highest temperature and may correlate with higher volatile contents, and therefore the greatest potential for decompression-driven explosive fragmentation. However, they are short lived and low volume following vent-clearing eruptions or collapses until conditions for blocky lava flows again prevail.

(2) Blocky lava flows produce regular small collapses from the flow fronts and flow sides. The higher volume the flow (i.e., the higher the extrusion rate), the greater the hazard potential. Flow fronts of long flows may collapse to form block and ash flows such as in September 1976 (Rose et al., 1976). In addition, large eruptions historically occur during an increase in extrusion rate and blocky lava flow development (i.e., November 1929, April 1973, November 2012). Loose debris associated with large volume flows is transported down river channels by destructive lahars (Harris et al., 2006).

(3) Spines are cooler and degassed prior to extrusion and collapse regularly along fractures during growth, producing a broad talus blanket and historically only small volume block and ash flows. Spines may be destroyed by subsequent vent-clearing eruptions.

Eruptions, small pyroclastic flows and collapses are associated with all lava types. However, the trends presented above provide an added understanding on the development of lava types and sequencing useful in continued hazard forecasting.

AUTHOR CONTRIBUTIONS

ER undertook field mapping and sample collection, compiled the timeline, and carried out textural analysis; BK and ER conceptualized models and wrote/edited the final manuscript; YL assisted with the field campaign provided constructive reviews on/edited the final manuscript; AH assisted with field work; ME assisted with tomography processing; GC was our scientific liaison in Guatemala and provided access to the domes.

FUNDING

We acknowledge financial support from the European Research Council (ERC) Starting Grant on Strain Localisation in Magma (SLiM, no. 306488). BK also acknowledges Marsden fast start grant (09-UO-017C), the science linkage funds [BMBF (grant NZL 09/17) in Germany and ISAT (grant E613) in New-Zealand] and the Medical Imaging beamline at the Australian Synchrotron, Victoria.

ACKNOWLEDGMENTS

We wish to thank Jeffrey Johnson, Benjamin Andrews, and Benjamin Philips for a great time in the field, support and discussion, and especially, Armando Pineda, without whom such challenging fieldwork could not have been accomplished so smoothly. We would also like to thank Bill Rose for constructive reviews of the initial MSc thesis. This research was undertaken on the IMBL beamlines at the Australian Synchrotron, Victoria, Australia. We would like to thank the beamline scientists for their technical help. This work was supported by the Multi-modal Australian ScienceS Imaging and Visualization Environment (MASSIVE) (www.massive.org.au).

REFERENCES

Anderson, S. W., and Fink, J. H. (1989). Hydrogen-isotope evidence for extrusion mechanisms of the Mt St. Helens lava dome. *Nature* 341, 521–523.

Anderson, S. W., and Fink, J. H. (1990). "The development and distribution of surface textures at the Mt St. Helens dome," in *Lava Flows and Domes: Emplacement Mechanisms and Hazard Implications, IAVCEI Proceedings in Volcanology, Vol. 2*,ed J. H. Fink (Berlin: Springer-Verlag), 25–46.

Anderson, S. W., and Fink, J. H. (1992). Crease structures: indicators of emplacement rates and surface stress regimes of lava flows. *Geol. Soc. Am. Bull.* 104, 615–625. doi: 10.1130/0016-7606(1992)104<0615:CSIOER>2.3.CO;2

Anderson, S. W., Fink, J. H., and Rose, W. I. (1995). Mount St. Helens and Santiaguito lava domes: the effect of short-term eruption rate on surface texture and degassing processes. *J. Volcanol. Geotherm. Res.* 69, 105–116. doi: 10.1016/0377-0273(95)00022-4

Andres, R., and Rose, W. I. (1995). Description of thermal anomalies on two active Guatemalan volcanoes using Landsat thematic mapper imagery. *Photogramm. Eng. Remote Sens.* 61, 775–782.

Andrews, B. J. (2014). Magmatic storage conditions, decompression rate, and incipient caldera collapse of the 1902 eruption of Santa Maria Volcano, Guatemala. *J. Volcanol. Geotherm. Res.* 282, 103–114. doi: 10.1016/j.jvolgeores.2014.06.009

Ashwell, P. A., Kendrick, J. E., Lavallée, Y., Kennedy, B. M., Hess, K.-U., von Aulock, F. W., et al. (2015). Permeability of compacting porous lavas. *J. Geophys. Res. Solid Earth* 120, 1605–1622. doi: 10.1002/2014JB011519

Avard, G., and Whittington, A. G. (2012). Rheology of arc dacite lavas: experimental determination at low strain rates. *Bull. Volcanol.* 74, 1039–1056. doi: 10.1007/s00445-012-0584-2

Ball, J. L., Calder, E. S., Hubbard, B. E., and Bernstein, M. L. (2013). An assessment of hydrothermal alteration in the Santiaguito lava dome complex,

Guatemala: implications for dome collapse hazards. *Bull. Volcanol.* 75:676. doi: 10.1007/s00445-012-0676-z

Bennati, L., Finizola, A., Walker, J. A., Lopez, D. L., Higuera-Diaz, I. C., Schütze, C., et al. (2011). Fluid circulation in a complex volcano-tectonic setting, inferred from self-potential and soil CO_2 flux surveys: the Santa María–Cerro Quemado–Zunil volcanoes and Xela caldera (Northwestern Guatemala). *J. Volcanol. Geotherm. Res.* 199, 216–229. doi: 10.1016/j.jvolgeores.2010.11.008

Bluth, G. J. S., and Rose, W. I. (2004). Observations of eruptive activity at Santiaguito volcano, Guatemala. *J. Volcanol. Geotherm. Res.* 136, 297–302. doi: 10.1016/j.jvolgeores.2004.06.001

Brill, K. A. (2011). *Characterization of Harmonic Tremor at Santiaguito Volcano and its Implications for Eruption Mechanisms*. Dissertation/masters's thesis, Michigan Technological University.

Calder, E. S., Lavallée, Y., Kendrick, J., and Bernstein, M. (2015). "Lava dome eruptions," in *Enyclopedia of Volcanoes 2nd Edn,* eds H. Sigurdsson, B. Houghton, H. Rymer, J. Stix, and S. McNutt (London, UK: Academic Press), 343–362.

Caricchi, L., Burlini, L., Ulmer, P., Gerya, T., Vassalli, M., and Papale, P. (2007). Non-newtonian rheology of crystal-bearing magmas and implications for magma ascent dynamics. *Earth Planet. Sci. Lett.* 264, 402–419. doi: 10.1016/j.epsl.2007.09.032

Caricchi, L., Pommier, A., Pistone, M., Castro, J., Burgisser, A., and Perugini, D. (2011). Strain-induced magma degassing: insights from simple-shear experiments on bubble bearing melts. *Bull. Volcanol.* 73, 1245–1257. doi: 10.1007/s00445-011-0471-2

Cashman, K. V., and Sparks, R. S. J. (2013). How volcanoes work: a 25 year perspective. *Geol. Soc. Am. Bull.* 125, 664–690. doi: 10.1130/B30720.1

Cashman, K. V., Sturtevant, B., Papale, P., and Navon, O. (2000). "Magmatic fragmentation," in *Encyclopedia of Volcanoes,* eds H. Sigurdsson, B. Houghton, H. Rymer, J. Stix, and S. McNutt (Waltham, MA: Academic Press), 459–471.

Castro, J. M., Cordonnier, B., Tuffen, H., Tobin, M. J., Puskar, L., Martin, M. C., et al. (2012). The role of melt-fracture degassing in defusing explosive rhyolite eruptions at volcán Chaitén. *Earth Planet. Sci. Lett.* 333–334, 63–69. doi: 10.1016/j.epsl.2012.04.024

Conway, F. M., Diehl, J. F., Rose, W. I., Matías, O., and Matias, O. (2013). Age and magma flux of Santa Maria Volcano, Guatemala: correlation of paleomagnetic waveforms with the 28,000 to 25,000 yr B.P. Mono Lake excursion. *J. Geol.* 102, 11–24. doi: 10.1086/629645

Cordonnier, B., Hess, K.-U., Lavallée, Y., and Dingwell, D. B. (2009). Rheological properties of dome lavas: case study of Unzen volcano. *Earth Planet. Sci. Lett.* 279, 263–272. doi: 10.1016/j.epsl.2009.01.014

De Angelis, S., Lamb, O. D., Lamur, A., Hornby, A. J., von Aulock, F. W., Chigna, G., et al. (2016). Characterization of moderate ash-and-gas explosions at Santiaguito volcano, Guatemala, from infrasound waveform inversion and thermal infrared measurements. *Geophys. Res. Lett.* 43, 6220–6227. doi: 10.1002/2016GL069098

Duffield, W., Heiken, G., Foley, D., and McEwen, A. (1993). Oblique synoptic images, produced from digital data, display strong evidence of a "new" caldera in southwestern Guatemala. *J. Volcanol. Geotherm. Res.* 55, 217–224.

Ebmeier, S. K., Biggs, J., Mather, T. A., Elliott, J. R., Wadge, G., and Amelung, F. (2012). Measuring large topographic change with InSAR: lava thicknesses, extrusion rate and subsidence rate at Santiaguito volcano, Guatemala. *Earth Planet. Sci. Lett.* 335–336, 216–225. doi: 10.1016/j.epsl.2012.04.027

Edmonds, M., and Herd, R. A. (2007). A volcanic degassing event at the explosive-effusive transition. *Geophys. Res. Lett.* 34:L21310. doi: 10.1029/2007GL031379

Eichelberger, J. C., Carrigan, C. R., Westrich, H. R., and Price, R. H. (1986). Non-explosive silicic volcanism. *Nature* 323, 598–602. doi: 10.1038/323598a0

Escobar-Wolf, R., Matias Gomez, R. O., and Rose, W. I. (2010). *Geologic Map of Santiaguito Volcano, Guatemala*. Geological Society of America Digital Map and Chart Series 8.

Fink, J. H., and Griffiths, R. W. (1998). Morphology, eruption rates, and rheology of lava domes: insights from laboratory models. *J. Geophys. Res.* 103, 527–545. doi: 10.1029/97JB02838

Fink, J. H., and Kieffer, S. W. (1993). Estimate of pyroclastic flow velocities resulting from explosive decompression of lava domes. *Nature* 363, 612–615. doi: 10.1038/363612a0

Fink, J. H., Malin, M. C., and Anderson, S. W. (1990). Intrusive and extrusive growth of the Mount St Helens lava dome. *Nature* 348, 435–437. doi: 10.1038/348435a0

Forbes, C. C. (2010). *Surficial Behavior of Lava Extruded by Santiaguito Dome, Guatemala, During January 2007 and January 2009*. Dissertation/master's thesis, Institute of Mining and Technology.

Gaunt, H. E., Sammonds, P. R., Meredith, P. G., Smith, R., and Pallister, J. S. (2014). Pathways for degassing during the lava dome eruption of Mount St. Helens 2004–2008. *Geology* 42, 947–950. doi: 10.1130/G35940.1

Ghiorso, M. S., and Sack, R. O. (1991). Mineralogy and Fe-Ti oxide geothermometry: thermodynamic formulation and the estimation of intensive variables in silicic magmas. *Contrib. Mineral. Petrol.* 108, 485–510. doi: 10.1007/BF00303452

Giordano, D., Russell, J. K., and Dingwell, D. B. (2008). Viscosity of magmatic liquids: a model. *Earth Planet. Sci. Lett.* 271, 123–134. doi: 10.1016/j.epsl.2008.03.038

Gonnermann, H. M., and Manga, M. (2007). The fluid mechanics inside a volcano. *Annu. Rev. Fluid Mech.* 39, 321–356. doi: 10.1146/annurev.fluid.39.050905.110207

Hale, A. J., and Wadge, G. (2008). The transition from endogenous to exogenous growth of lava domes with the development of shear bands. *J. Volcanol. Geotherm. Res.* 171, 237–257. doi: 10.1016/j.jvolgeores.2007.12.016

Hammer, J. E., Cashman, K. V., and Voight, B. (2000). Magmatic processes revealed by textural and compositional trends in Merapi dome lavas. *J. Volcanol. Geotherm. Res.* 100, 165–192. doi: 10.1016/S0377-0273(00)00136-0

Harris, A. J., Flynn, L. P., Matias, O., Rose, W. I., and Cornejo, J. (2004). The evolution of an active silicic lava flow field: an ETM+ perspective. *J. Volcanol. Geotherm. Res.* 135, 147–168. doi: 10.1016/j.jvolgeores.2003.12.011

Harris, A. J. L., Flynn, L. P., Matias, O., and Rose, W. I. (2002). The thermal stealth flows of Santiaguito dome, Guatemala: implications for the cooling and emplacement of dacitic block-lava flows. *GSA Bull.* 114, 533–546. doi: 10.1130/0016-7606(2002)114<0533:TTSFOS>2.0.CO;2

Harris, A. J. L., Rose, W. I., and Flynn, L. P. (2003). Temporal trends in lava dome extrusion at Santiaguito 1922-2000. *Bull. Volcanol.* 65, 77–89. doi: 10.1007/s00445-002-0243-0

Harris, A. J. L., Vallance, J. W., Rose, W. I., Kimberly, P., and Flynn, L. P. (2006). Downstrean aggradation owing to lava dome extrusion and rainfall runoff at Volcán Santiaguito, Guatemala. *Geol. Soc. Am. Spec. Pap.* 412, 86–104. doi: 10.1130/2006.2412(05)

Holland, A. S. P., Watson, I. M., Phillips, J. C., Caricchi, L., and Dalton, M. P. (2011). Degassing processes during lava dome growth: insights from Santiaguito lava dome, Guatemala. *J. Volcanol. Geotherm. Res.* 202, 153–166. doi: 10.1016/j.jvolgeores.2011.02.004

Hornby, A. J., Kendrick, J. E., Lamb, O. D., Hirose, T., De Angelis, S., von Aulock, F. W., et al. (2015). Spine growth and seismogenic faulting at Mt. Unzen, Japan. *J. Geophys. Res. Solid Earth* 120, 4034–4054. doi: 10.1002/2014JB011660

Jaupart, C., and Allègre, C. J. (1991). Gas content, eruption rate and instabilities of eruption regime in silicic volcanoes. *Earth Planet. Sci. Lett.* 102, 413–429. doi: 10.1016/0012-821X(91)90032-D

Johnson, J. B. (2004). Explosion dynamics of pyroclastic eruptions at Santiaguito Volcano. *Geophys. Res. Lett.* 31, 1–5. doi: 10.1029/2003GL019079

Kendrick, J. E., Lavallée, Y., Ferk, A., Perugini, D., Leonhardt, R., and Dingwell, D. B. (2012). Extreme frictional processes in the volcanic conduit of Mount St. Helens (USA) during the 2004–2008 eruption. *J. Struct. Geol.* 38, 61–76. doi: 10.1016/j.jsg.2011.10.003

Kendrick, J. E., Lavallée, Y., Hess, K.-U., Heap, M. J., Gaunt, H. E., Meredith, P. G., et al. (2013). Tracking the permeable porous network during strain-dependent magmatic flow. *J. Volcanol. Geotherm. Res.* 260, 117–126. doi: 10.1016/j.jvolgeores.2013.05.012

Kendrick, J. E., Lavallée, Y., Hirose, T., Di Toro, G., Hornby, A. J., De Angelis, S., et al. (2014). Volcanic drumbeat seismicity caused by stick-slip motion and magmatic frictional melting. *Nat. Geosci.* 7, 438–442. doi: 10.1038/ngeo2146

Kendrick, J. E., Lavallée, Y., Varley, N. R., Wadsworth, F. B., Lamb, O. D., and Vasseur, J. (2016). Blowing off steam: tuffisite formation as a regulator for lava Dome eruptions. *Front. Earth Sci.* 4:41. doi: 10.3389/feart.2016.00041

Kennedy, B. M., Wadsworth, F. B., Vasseur, J., Ian Schipper, C., Mark Jellinek, A., von Aulock, F. W., et al. (2016). Surface tension driven processes densify and retain permeability in magma and lava. *Earth Planet. Sci. Lett*. 433, 116–124. doi: 10.1016/j.epsl.2015.10.031

Lavallée, Y., Benson, P. M., Heap, M. J., Hess, K. U., Flaws, A., Schillinger, B., et al. (2013). Reconstructing magma failure and the degassing network of dome-building eruptions. *Geology* 41, 515–518. doi: 10.1130/G33948.1

Lavallée, Y., Dingwell, D. B., Johnson, J. B., Cimarelli, C., Hornby, A. J., Kendrick, J. E., et al. (2015). Thermal vesiculation during volcanic eruptions. *Nature* 528, 544–547. doi: 10.1038/nature16153

Lavallée, Y., Hess, K. U., Cordonnier, B., and Dingwell, B. D. (2007). Non-Newtonian rheological law for highly crystalline dome lavas. *Geology* 35:843. doi: 10.1130/G23594A.1

MacKay, M. E., Rowland, S. K., Mouginis-Mark, P. J., and Garbeil, H. (1998). Thick lava flows of Karisimbi Volcano, Rwanda: insights from SIR-C interferometric topography. *Bull. Volcanol*. 60, 239–251. doi: 10.1007/s004450050230

Manley, C. R. (1996). Physical volcanology of a voluminous rhyolite lava flow: the Badlands lava, Owyhee Plateau, Southwestern Idaho. *J. Volcanol. Geotherm. Res*. 71, 129–153. doi: 10.1016/0377-0273(95)00066-6

Manley, C. R., and Fink, J. H. (1987). Internal textures of rhyolite flows as revealed by research drilling. *J. Geol.* 15, 549–522. doi: 10.1130/0091-7613(1987)15<549:ITORFA>2.0.CO;2

Mueller, S., Llewellin, E. W., and Mader, H. M. (2009). The rheology of suspensions of solid particles. *Proc. R. Soc. A Math. Phys. Eng. Sci*. 466, 1201–1228. doi: 10.1098/rspa.2009.0445

Mueller, S., Scheu, B., Kueppers, U., Spieler, O., Richard, D., and Dingwell, D. B. (2011). The porosity of pyroclasts as an indicator of volcanic explosivity. *J. Volcanol. Geotherm. Res*. 203, 168–174. doi: 10.1016/j.jvolgeores.2011.04.006

Nakada, S., and Motomura, Y. (1999). Petrology of the 1991–1995 eruption at Unzen: effusion pulsation and groundmass crystallization. *J. Volcanol. Geotherm. Res*. 89, 173–196. doi: 10.1016/S0377-0273(98)00131-0

Nakada, S., Shimizu, H., and Ohta, K. (1999). Overview of the 1990–1995 eruption at Unzen Volcano. *J. Volcanol. Geotherm. Res*. 89, 1–22. doi: 10.1016/S0377-0273(98)00118-8

Navarro-Ochoa, C., Gavilanes-Ruiz, J. C., and Cortés-Cortés, A. (2002). Movement and emplacement of lava flows at Volcan de Colima, Mexico: november 1998 – February 1999. *J. Volcanol. Geotherm. Res*. 117, 155–167. doi: 10.1016/S0377-0273(02)00242-1

Okumura, S., Nakamura, M., Takeuchi, S., Tsuchiyama, A., Nakano, T., and Uesugi, K. (2009). Magma deformation may induce non-explosive volcanism via degassing through bubble networks. *Earth Planet. Sci. Lett*. 281, 267–274. doi: 10.1016/j.epsl.2009.02.036

Pallister, J. S., Cashman, K. V., Hagstrum, J. T., Beeler, N. M., Moran, S. C., and Denlinger, R. P. (2012). Faulting within the Mount St. Helens conduit and implications for volcanic earthquakes. *Geol. Soc. Am. Bull*. 125, 359–376. doi: 10.1130/B30716.1

Ridolfi, F., Renzulli, A., and Puerini, M. (2010). Stability and chemical equilibrium of amphibole in calc-alkaline magmas: an overview, new thermobarometric formulations and application to subduction-related volcanoes. *Contrib. Mineral. Petrol*. 160, 45–66. doi: 10.1007/s00410-009-0465-7

Rose, W. I. (1972a). Notes on the 1902 eruption of Santa María volcano, Guatemala. *Bull. Volcanol*. 36, 29–45.

Rose, W. I. (1972b). Santiaguito Volcanic Dome, Guatemala. *Geol. Soc. Am. Bull*. 83, 1413–1434.

Rose, W. I. (1973a). Nuée ardente from Santiaguito Volcano April 1973. *Bull. Volcanol*. 37, 365–371.

Rose, W. I. (1973b). Pattern and mechanism of volcanic activity at the Santiaguito Volcanic Dome, Guatemala. *Bull. Volcanol*. 37, 73–94.

Rose, W. I. (1987a). Santa María, Guatemala: bimodal soda-rich calc-alkalic stratovolcano. *J. Volcanol. Geotherm. Res*. 33, 109–129.

Rose, W. I. (1987b). "Volcanic activity at Santiaguito Volcano 1976-1984," in *The Emplacement of Silicic Domes and Lava Flows. Geological Society of America Special Paper 212*, ed J. H. Fink (Boulder, CO: The Geolgical Society of America), 17–27.

Rose, W. I., Grant, N. K., Hahn, G. A., Lange, I. M., Powell, J. L., Easter, J., et al. (1977). The evolution of Santa María Volcano. *J. Geol*. 85, 63–87. doi: 10.1086/628269

Rose, W. I., Pearson, T., and Bonis, S. (1976). Nuée ardente eruption from the foot of a dacite lava flow, Santiaguito Volcano, Guatemala. *Bull. Volcanol*. 40, 23–38. doi: 10.1007/BF02599827

Rose, W. I., Stoiber, R. E., and Bonis, S. B. (1970). Volcanic activity at Santiaguito Volcano, Guatemala June 1968 – August 1969. *Bull. Volcanol*. 34, 295–307. doi: 10.1007/BF02597792

Rust, A. C., and Cashman, K. V. (2011). Permeability controls on expansion and size distributions of pyroclasts. *J. Geophys. Res*. 116, 1–17. doi: 10.1029/2011JB008494

Rust, A. C., Manga, M., and Cashman, K., V (2003). Determining flow type, shear rate and shear stress in magmas from bubble shapes and orientations. *J. Volcanol. Geotherm. Res*. 122, 111–132. doi: 10.1016/S0377-0273(02)00487-0

Sahetapy-Engel, S. T., and Harris, A. J. L. (2008). Thermal structure and heat loss at the summit crater of an active lava dome. *Bull. Volcanol*. 71, 15–28. doi: 10.1007/s00445-008-0204-3

Sahetapy-Engel, S. T., Harris, A. J. L., and Marchetti, E. (2008). Thermal, seismic and infrasound observations of persistent explosive activity and conduit dynamics at Santiaguito lava dome, Guatemala. *J. Volcanol. Geotherm. Res*. 173, 1–14. doi: 10.1016/j.jvolgeores.2007.11.026

Sahetapy-Engel, S. T. M., Flynn, L. P., and Harris, A. J. L. (2004). Surface temperature and spectral measurements at Santiaguito lava dome, Guatemala. *Geophys. Res. Lett*. 31:L19610. doi: 10.1029/2004GL020683

Sanderson, R. W., Johnson, J. B., and Lees, J. M. (2010). Ultra-long period seismic signals and cyclic deflation coincident with eruptions at Santiaguito volcano, Guatemala. *J. Volcanol. Geotherm. Res*. 198, 35–44. doi: 10.1016/j.jvolgeores.2010.08.007

Sapper, K. (1926). Die Vulkanische tatigkeit in mittelamerika im 20 jahrhundert. *Zeitschrift fuer Vulkanol*. 9, 156–203.

Scaillet, B., Clemente, B., Evans, B., and Pichavant, M. (1998). Redox control of sulfur degassing in silicic magmas. *J. Geophys. Res*. 103, 937–949. doi: 10.1029/98JB02301

Scharff, L., Ziemen, F., Hort, M., Gerst, A., and Johnson, J. B. (2012). A detailed view into the eruption clouds of Santiaguito volcano, Guatemala, using Doppler radar. *J. Geophys. Res*. 117, 1–21. doi: 10.1029/2011JB008542

Schneider, D., and Vallance, J. (2008). "Use of thermal infrared imaging for monitoring renewed dome growth at Mount St. Helens, 2004," in *A Volcano Rekindled: The Renewed Eruption of Mount St. Helens, 2004–2006 (US. Geological Survey Professional Paper 1750)*, 347–359.

Scott, J. A. J., Mather, T. A., Pyle, D. M., Rose, W. I., and Chigna, G. (2012). The magmatic plumbing system beneath Santiaguito Volcanco, Guatemala. *J. Volcanol. Geotherm. Res*. 237–238, 54–68. doi: 10.1016/j.jvolgeores.2012.05.014

Scott, J. A. J., Pyle, D. M., Mather, T. A., and Rose, W. I. (2013). Geochemistry and evolution of the Santiaguito volcanic dome complex, Guatemala. *J. Volcanol. Geotherm. Res*. 252, 92–107. doi: 10.1016/j.jvolgeores.2012.11.011

Simkin, T., Sibert, L., and Kimberly, P. (1994). *Volcanoes of the World*. Oakland, CA: University of California Press.

Singer, B. S., Jicha, B. R., Fournelle, J. H., Beard, B. L., Johnson, C. M., Smith, K. E., et al. (2013). Lying in wait: deep and shallow evolution of dacite beneath Volcan de Santa Maria, Guatemala. *Geol. Soc. Lond. Spec. Publ*. 385, 209–234. doi: 10.1144/SP385.2

Singer, B. S., Smith, K. E., Jicha, B. R., Beard, B. L., Johnson, C. M., and Rogers, N. W. (2011). Tracking open-system differentiation during growth of Santa Maria Volcano, Guatemala. *J. Petrol*. 52, 2335–2363. doi: 10.1093/petrology/egr047

Smith, J. V., Miyake, Y., and Oikawa, T. (2001). Interpretation of porosity in dacite lava domes as ductile-brittle failure textures. *J. Volcanol. Geotherm. Res*. 112, 25–35. doi: 10.1016/S0377-0273(01)00232-3

Smithsonian Institution (1980). *Santa Maria*. Scientific Event Alert Network Bull. Washington, DC: Smithsonian Institution.

Sparks, R. (2003). Dynamics of magma degassing. *Geol. Soc. Lond. Spec. Publ*. 213, 5–22. doi: 10.1144/GSL.SP.2003.213.01.02

Stoiber, R. E., and Rose, W. I. (1969). Recent volcanic and fumarolic activity at Santiaguito volcano, Guatemala. *Bull. Volcanol*. 33, 475–502. doi: 10.1007/BF02596520

Stoiber, R. E., and Rose, W. I. (1970). The geochemistry of Central American volcanic gas condensates. *Geol. Soc. Am. Bull*. 81, 2891–2912. doi: 10.1130/0016-7606(1970)81[2891:TGOCAV]2.0.CO;2

Swanson, D. A., and Holcomb, T. T. (1990). "Regularities in growth of the Mount St. Helens dacite dome, 1980–1986," in *Lava Flows and Domes: Emplacement Mechanisms and Hazard Implications,* ed J. H. Fink (Berlin; Heidelberg: Springer), 3–24.

Tuffen, H., Dingwell, D., and Pinkerton, H. (2003). Repeated fracture and healing of silicic magma generate flow banding and earthquakes? *Geology* 31, 1089–1092. doi: 10.1130/G19777.1

Tuffen, H., James, M. R., Castro, J. M., and Schipper, C. I. (2013). Exceptional mobility of an advancing rhyolitic obsidian flow at Cordón Caulle volcano in Chile. *Nat. Commun.* 4:2709. doi: 10.1038/ncomms3709

Wadge, G., Ryan, G., and Calder, E. S. (2009). Clastic and core lava components of a silicic lava dome. *Geology* 37, 551–554. doi: 10.1130/G25747A.1

Watts, R. B., Herd, R. A., Sparks, R. S. J., and Young, S. R. (2002). Growth patterns and emplacement of the andesitic lava dome at Soufriere Hills Volcano, Montserrat. *Geol. Soc. Lond. Mem*. 21, 115–152. doi: 10.1144/GSL.MEM.2002.021.01.06

Williams, H. (1932). The history and character of volcanic domes. *Univ. Calif. Publ. Geol. Sci*. 21, 51–146.

Williams, S. N., and Self, S. (1983). The October 1902 Plinian eruption of Santa Maria Volcano, Guatemala. *J. Volcanol. Geotherm. Res*. 16, 33–56. doi: 10.1016/0377-0273(83)90083-5

Wright, H. M. N., Roberts, J. J., and Cashman, K. V. (2006). Permeability of anisotropic tube pumice: model calculations and measurements. *Geophys. Res. Lett*. 33:L17316. doi: 10.1029/2006GL027224

Zobin, V., Luhr, J., Taran, Y., Bretón, M., Cortés, A., De La Cruz-Reyna, S., et al. (2002). Overview of the 1997–2000 activity of Volcán de Colima, México. *J. Volcanol. Geotherm. Res*. 117, 1–19. doi: 10.1016/S0377-0273(02)00232-9

Conflict of Interest Statement: The authors declare that the research was conducted in the absence of any commercial or financial relationships that could be construed as a potential conflict of interest.

The reviewer, MC, and handling editor declared their shared affiliation.